JACS
JOURNAL OF THE AMERICAN CHEMICAL SOCIETY
Article
pubs.acs.org/JACS

Ternary Hybrid Material for High-Performance Lithium−Sulfur Battery

Qi Fan,[†,‡] Wen Liu,[†] Zhe Weng,[†] Yueming Sun,[‡] and Hailiang Wang*[,†]

[†]Department of Chemistry and Energy Sciences Institute, Yale University, New Haven, Connecticut 06511, United States
[‡]School of Chemistry and Chemical Engineering, Southeast University, Nanjing, Jiangsu 211189, China

Supporting Information

ABSTRACT: The rechargeable lithium−sulfur battery is a promising option for energy storage applications because of its low cost and high energy density. The electrochemical performance of the sulfur cathode, however, is substantially compromised because of fast capacity decay caused by polysulfide dissolution/shuttling and low specific capacity caused by the poor electrical conductivities of the active materials. Herein we demonstrate a novel strategy to address these two problems by designing and synthesizing a carbon nanotube (CNT)/$NiFe_2O_4$−S ternary hybrid material structure. In this unique material architecture, each component synergistically serves a specific purpose: The porous CNT network provides fast electron conduction paths and structural stability. The $NiFe_2O_4$ nanosheets afford strong binding sites for trapping polysulfide intermediates. The fine S nanoparticles well-distributed on the CNT/$NiFe_2O_4$ scaffold facilitate fast Li^+ storage and release for energy delivery. The hybrid material exhibits balanced high performance with respect to specific capacity, rate capability, and cycling stability with outstandingly high Coulombic efficiency. Reversible specific capacities of 1350 and 900 mAh g^{-1} are achieved at rates of 0.1 and 1 C respectively, together with an unprecedented cycling stability of ∼0.009% capacity decay per cycle over more than 500 cycles.

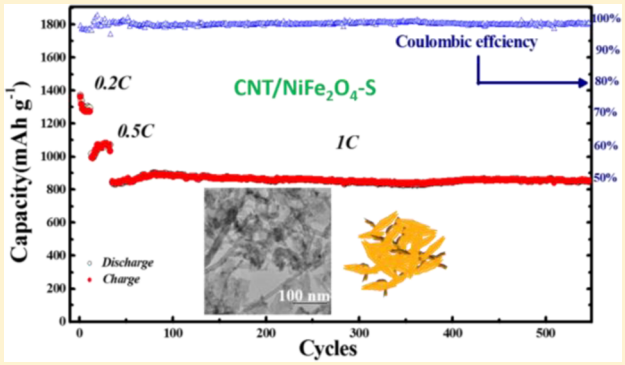

INTRODUCTION

With the rapid development of modern society and the increasing demand for energy consumption, battery systems for propelling electric vehicles and storing surplus electricity generated from renewable sources have attracted considerable attention during the past decade.[1−3] More powerful and durable batteries with high energy density and long cycle life are highly desired. Lithium-ion batteries, which dominates today's portable electronics and consumer product markets, have encountered their theoretical energy-density limit.[1,4,5] The lithium−sulfur battery, a "beyond lithium ion" technology, is considered to be a promising candidate for the next generation of rechargeable batteries because its theoretical specific energy is several times higher than that of the lithium-ion battery.[4,6,7]

Sulfur, one of the most abundant elements in the earth's crust, has a high theoretical specific capacity of 1675 mAh g^{-1} as the cathode material in lithium−sulfur batteries, making it useful for high-energy-demand applications such as electric transportation.[4] Sulfur is also an inexpensive and environmentally friendly material, which is beneficial to large-scale stationary energy storage assuming high efficiency and long cycle life are achieved.[6,7] However, several challenges associated with sulfur cathode materials still persist and may prevent their practical applications, including (i) low electronic and ionic conductivities of solid sulfur species (S, Li_2S_2, and Li_2S) that limit specific capacity and rate capability,[8−11] (ii) dissolution of polysulfide intermediates into electrolyte and subsequent redox shuttling resulting in low Coulombic efficiency, rapid capacity fading, and high self-discharge rates,[12−15] and (iii) significant volumetric changes (∼80%) during charging and discharging reactions that may induce mechanical damage to the electrode.[16,17]

Various strategies have thus far been used to improve the material structures of sulfur electrodes. Nanocarbons including carbon nanospheres, carbon nanofibers, graphene sheets, carbon nanotubes (CNTs), and meso-/microporous carbons have been made into composite materials with sulfur by physical mixing, chemical assembly, direct growth, or in situ carbonization. This strategy not only improves the electrical conductivity of the electrode but also provides pore structures to accommodate volumetric changes during cycling.[11,18−26] However, carbon hybridization is less effective in trapping polysulfides because the chemical interactions between the nonpolar carbons and the polar polysulfides are rather weak.[13,27] Recently, metal oxides and chalcogenides have been introduced into the electrode for their strong binding of polysulfides, resulting in considerable gains in Coulombic efficiency and cycling stability.[13,28−33] Although some of the oxides and chalcogenides are considered electrically conductive,

Received: July 7, 2015
Published: September 17, 2015

DOI: 10.1021/jacs.5b07071
J. Am. Chem. Soc. 2015, 137, 12946−12953

they are still less conductive than graphitic carbons by orders of magnitude, which may lead to undesirable compromises in specific capacity and rate performance.

To address the challenges further, our strategy is to utilize ternary hybrid material structures where one component is used for electron conduction and a second component is used for polysulfide immobilization. We demonstrate this idea with a CNT/$NiFe_2O_4$–S hybrid material. $NiFe_2O_4$ nanosheets are anchored on CNTs to form a carbon/inorganic scaffold to host nanosized S that is the active component for energy storage. The 1D CNTs form a highly conductive porous network for fast electron transport, mass diffusion, and structural stabilization.[34,35] The 2D metal oxide nanosheets provide strong binding sites for polysulfide intermediates and thus restrict shuttling. The nanosized S particles serve as the active material to deliver and store energy. As a result of the 3D ternary hybrid architecture, our material exhibits balanced high performance with respect to specific capacity, rate capability, and cycling stability. High reversible specific capacities of ~1350 and 900 mAh g^{-1} are achieved at rates of 0.1 and 1 C, respectively, with outstanding Coulombic efficiencies (higher than 99.2%) and a high sulfur content (~76%). The battery delivers unprecedented capacity retention over 500 cycles at 1 C with a decay as low as ~0.009% per cycle.

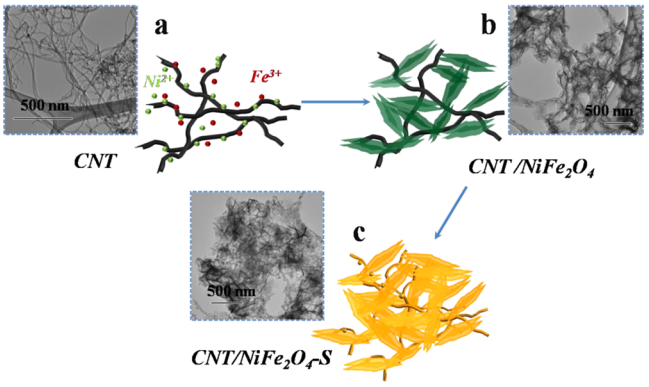

Figure 1. Schematic illustration of the synthesis process of the CNT/$NiFe_2O_4$–S ternary material structure. (a) Mildly oxidized multiwall CNTs mixed with $Ni(OAc)_2$ and $Fe(NO_3)_3$ in solution. (b) $NiFe_2O_4$ nanosheets grown on CNTs. (c) S deposited on the CNT/$NiFe_2O_4$ scaffold.

EXPERIMENTAL SECTION

Preparation of CNT/$NiFe_2O_4$. CNTs were oxidized following a modified Hummers method reported previously. (See Supporting Information for details.)[36] In a typical synthesis, 16 mg of mildly oxidized CNTs were dispersed in 16 mL of anhydrous N, N-dimethylformamide (DMF) assisted by sonication for 10 min. After that, 90 mg of methenamine was dissolved into the mixture with vigorously stirring for 5 min. Then, 800 μL of 0.2 M $Ni(OAc)_2$ and 800 μL of 0.2 M $Fe(NO_3)_3$ aqueous solutions were added. The mixture was vigorously stirred at 85 °C for 5 h and transferred to a 40 mL Teflon-lined stainless-steel autoclave for solvothermal reaction at 160 °C for 5 h. The final product was collected by centrifuge, repeatedly washed with water, and lyophilized. CNT/$NiFe_2O_4$-2 was synthesized using the same method except that 400 μL of 0.2 M $Ni(OAc)_2$ solution was used instead of 800 μL.

Preparation of CNT/$NiFe_2O_4$–S. A 30 mg amount of CNT/$NiFe_2O_4$ was dispersed in 100 mL of deionized water and 10 mL of absolute ethanol. A 100 mg amount of sublimed sulfur was dissolved in 4 mL of anhydrous ethylenediamine (EDA), which was then added dropwise into the CNT/$NiFe_2O_4$ dispersion under vigorous stirring. Then, 10% HNO_3 solution was added dropwise into the mixture until the pH reached 6–7 to precipitate S from its complex with EDA.[21] The suspension was continuously stirred overnight; then, the final product was obtained through filtration, rinsing, and drying

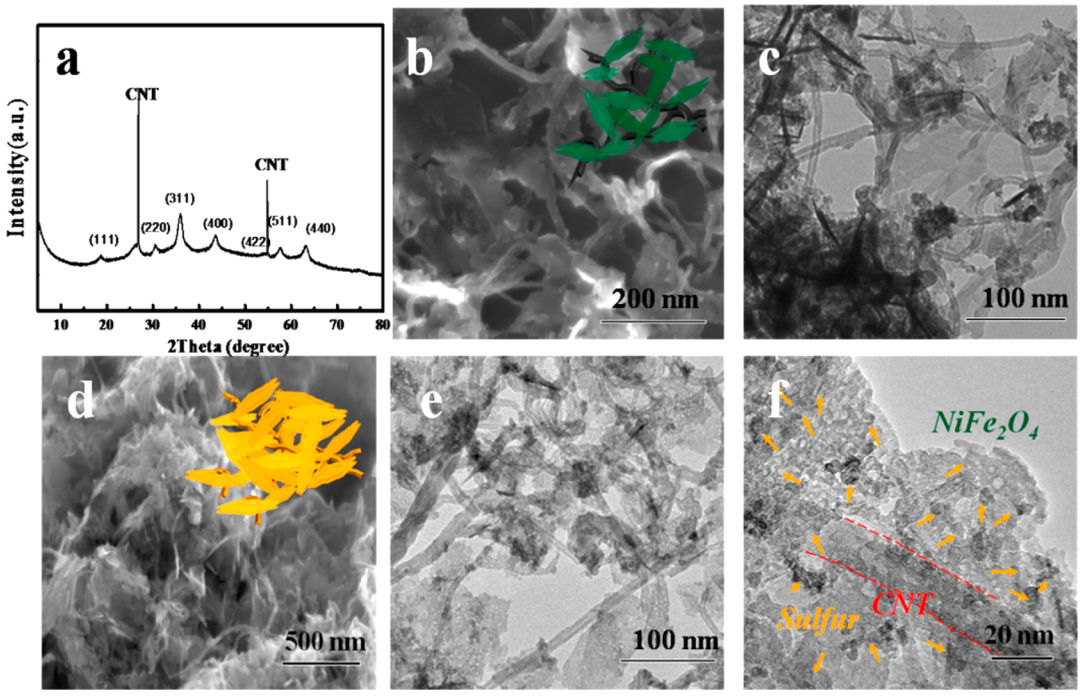

Figure 2. Structural characterizations of the CNT/$NiFe_2O_4$ binary scaffold and the CNT/$NiFe_2O_4$–S ternary hybrid material. (a) XRD pattern showing the phase composition of CNT/$NiFe_2O_4$. (b) SEM and (c) TEM images showing the morphology of CNT/$NiFe_2O_4$. (d) SEM and (e) TEM images showing the morphology of CNT/$NiFe_2O_4$–S. (f) High-magnification TEM image showing the fine S nanoparticles coating the surface of CNT/$NiFe_2O_4$.

DOI: 10.1021/jacs.5b07071
J. Am. Chem. Soc. 2015, 137, 12946–12953

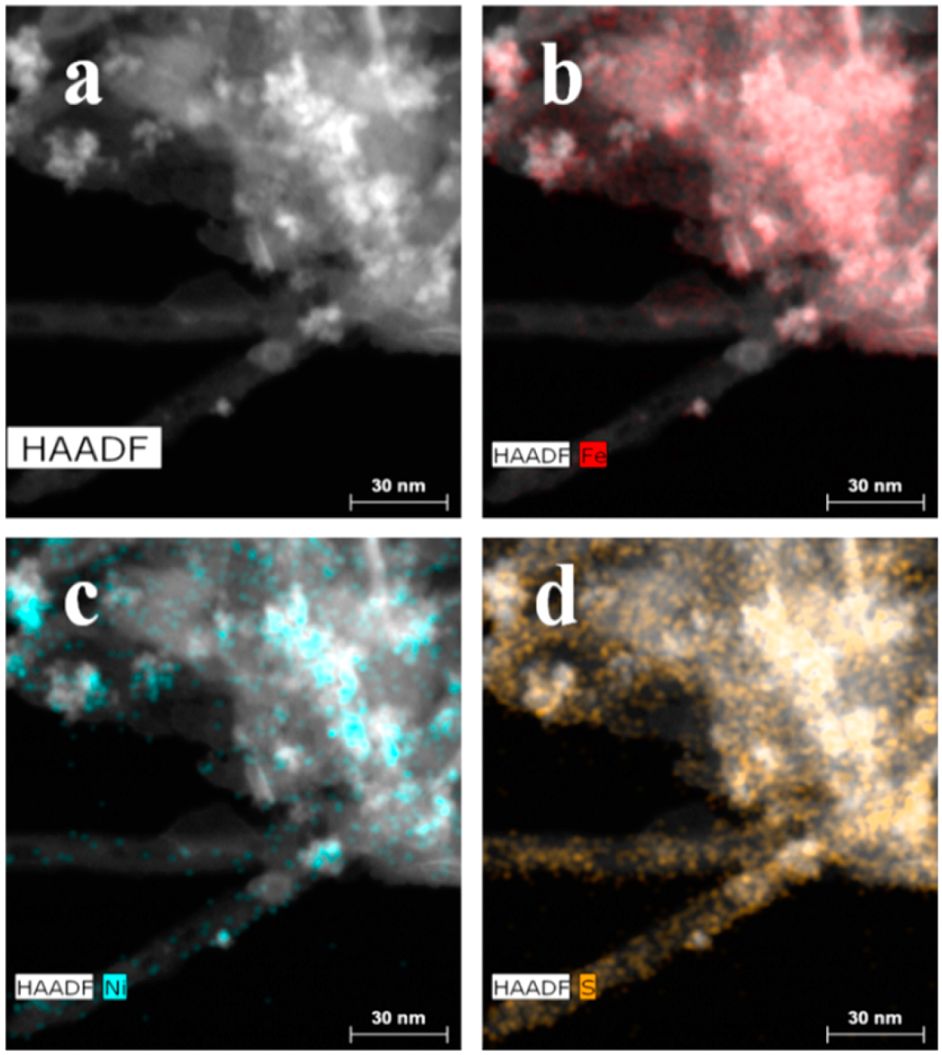

Figure 3. Maps of elements in the CNT/$NiFe_2O_4$−S ternary hybrid material. (a) STEM image of the selected region recorded by the high angle annular dark field (HAADF) detector. EDS maps of (b) Fe, (c) Ni, and (d) S elements in the selected region of the CNT/$NiFe_2O_4$−S ternary hybrid material.

at 60 °C under vacuum. CNT/$NiFe_2O_4$−S-2 and CNT−S were prepared in the same way using CNT/$NiFe_2O_4$-2 and CNT as host materials.

Electrochemical Measurements. Cathodes were prepared by casting the *N*-methyl-2-pyrrolidone (NMP) slurry containing CNT/$NiFe_2O_4$−S, Super P carbon, and polyvinylidene fluoride (PVDF) in the weight ratio of 72:12:16 onto an Al current collector. Average sulfur mass loading was between 1.0 and 1.2 mg cm^{-2}. Coin cells (2032 type) were assembled using lithium foil as the anode and Celgard 3501 sheets as the separator. The electrolyte was 1 M lithium bis(trifluoromethanesulfonyl)imide (LiTFSI) in a mixed solvent of 1,2-dimethoxyethane (DME) and 1,3-dioxolane (DOL) with a volumetric ratio of 1:1 with 2 wt % of $LiNO_3$. The electrolyte amount was 40 μL. The electrode area was 1.1 cm^2 (diameter of 12 mm). Electrochemical studies were carried out using MTI BST8-MA and Arbin BT2143 battery analyzers. Cells were operated in the voltage window of 1.7−2.6 V. Specific capacity values were calculated with respect to the mass of sulfur.

Structure Characterizations. X-ray diffraction (XRD) was performed with a Rigaku Smart LAB 3 diffractometer using Cu Kα radiation (40 kV, 100 mA, λ = 1.54 Å). The scanning electron microscopy (SEM) studies were carried out on a Hitachi SU-70 SEM instrument at 5 keV. Low-magnification transmission electron microscopy (TEM) images were taken with a JEOL JEM 1400 instrument at 80 keV. High-magnification TEM imaging and energy dispersive spectroscopy (EDS) mapping were performed on an FEI Tecnai Osiris TEM microscope at 200 keV.

RESULTS AND DISCUSSION

Results. *Structure Design and Material Synthesis.* Our synthesis approach to the CNT/$NiFe_2O_4$−S ternary hybrid material is first to build the CNT/$NiFe_2O_4$ binary structure and then to deposit S onto it (Figure 1). The CNT/$NiFe_2O_4$ was synthesized by directly and selectively growing $NiFe_2O_4$ nanosheets on CNTs using a two-step solution-phase method. In the first step, $Ni(OAc)_2$ and $Fe(NO_3)_3$ were hydrolyzed in the presence of mildly oxidized multiwall CNTs. Mixed solvents and a relatively low temperature (85 °C) were used so that the inorganic precursors could sufficiently interact with the oxygen functional groups on the CNT surface to trigger selective nucleation and subsequent uniform growth of the hydrolyzed products.[37,38] In the second step, solvothermal treatment was used to produce the final binary material.

The microstructure of the binary material was imaged with SEM and TEM. It was observed that nanosheets with irregular shapes were attached to CNTs forming a woven network (Figure 2b,c). The lateral size of the nanosheets is about 50−200 nm, and the thickness is less than 5 nm (Figure S1).

DOI: 10.1021/jacs.5b07071
J. Am. Chem. Soc. 2015, 137, 12946−12953

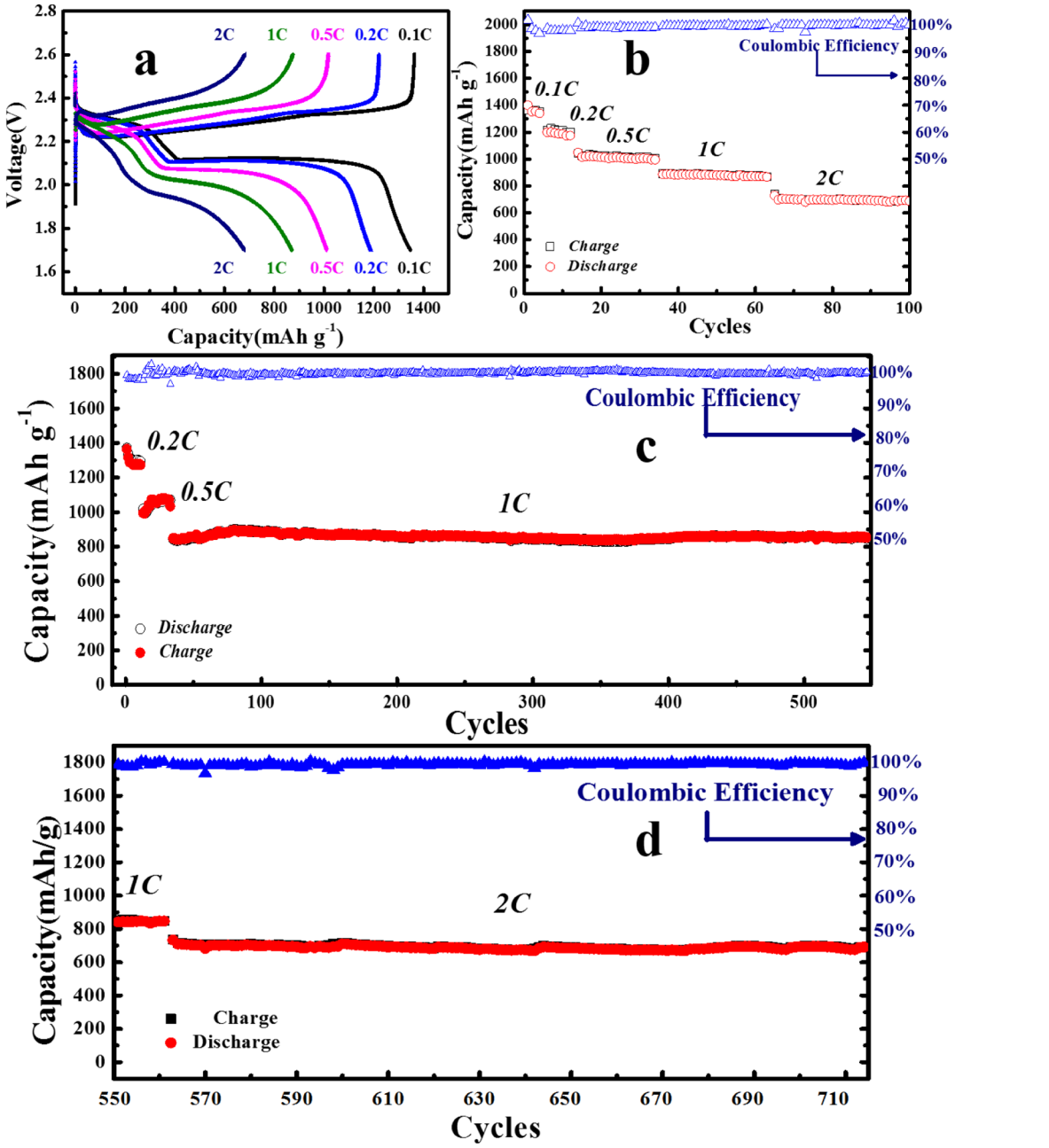

Figure 4. Electrochemical performance of Li–S batteries using the CNT/$NiFe_2O_4$–S ternary hybrid material as the cathode. (a) Representative charging/discharging voltage profiles of the CNT/$NiFe_2O_4$–S ternary hybrid at various *C* rates from 0.1 to 2 C. Specific capacity values were calculated on the basis of the mass of sulfur. (b) Rate performance of CNT/$NiFe_2O_4$–S with corresponding Coloumbic efficiency. (c) Long-term cycling stability test showing unprecedentedly high capacity retention with excellent Coloumbic efficiency over 500 cycles at 1 C. (d) Continued cycling performance of the CNT/$NiFe_2O_4$–S electrode (the same cell as for c) over 150 cycles at 2 C.

XRD analysis confirmed that the nanosheets were spinel-structured $NiFe_2O_4$ with *Fd*3*m* space group (Figure 2a). The CNT/$NiFe_2O_4$ material showed a BET surface area of ~192 m^2/g.

S was deposited onto the CNT/$NiFe_2O_4$ scaffold to generate the CNT/$NiFe_2O_4$–S hybrid material.[21] After the S deposition process, the ternary material maintained the morphology of the CNT/$NiFe_2O_4$ scaffold (Figure 2d,e), indicating that S was uniformly distributed on the surface of the structure. The S-coated $NiFe_2O_4$ nanosheets were closely wired by the interconnected CNTs. High-magnification TEM imaging provided more details about the S coating: S nanoparticles with small sizes were uniformly dispersed and formed a nanolayer on the surface of both the $NiFe_2O_4$ nanosheets and the CNTs within the ternary hybrid material structure. XRD measurement indicated the average size of the S nanoparticles is about 5–20 nm (Figure S3), consistent with the TEM observation.[21] The CNT/$NiFe_2O_4$–S contained ~76% of S by mass. The BET surface area of CNT/$NiFe_2O_4$–S is ~49 m^2/g. Because the sample was degassed at only 50 °C to avoid sulfur loss, the calculated specific surface area represents an estimate on the low end.

The distribution of the elements of interest in the ternary hybrid material architecture were further probed using EDS under scanning TEM (STEM) mode (Figure 3). Both Fe and Ni were observed to be well-dispersed within the nanosheets (Figure 3b,c),

DOI: 10.1021/jacs.5b07071
J. Am. Chem. Soc. 2015, 137, 12946–12953

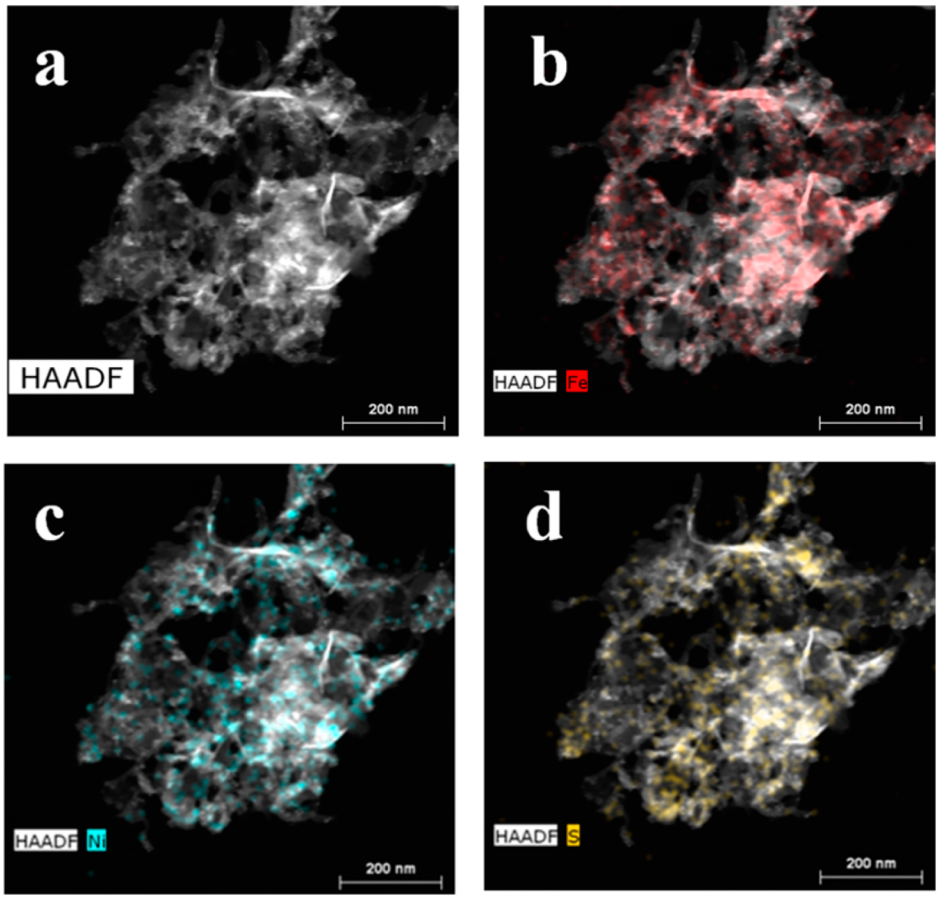

Figure 5. Maps of elements in the CNT/$NiFe_2O_4$–S ternary hybrid material after long-term cycling. (a) STEM image of the selected region. EDS maps of (b) Fe, (c) Ni, and (d) S in the selected regions of the cycled CNT/$NiFe_2O_4$–S ternary hybrid material.

suggesting the nanosheets are indeed a mixed oxide of Fe and Ni. It is also evident that the $NiFe_2O_4$ nanosheets are well-anchored on the CNTs. Mapping of S revealed that S is uniformly distributed on the surfaces of both the $NiFe_2O_4$ nanosheets and the CNTs (Figure 3d), consistent with the TEM imaging results.

Electrochemical Properties and Battery Performance. The CNT/$NiFe_2O_4$–S ternary material was made into coin-cell-type batteries and cycled between 1.7 and 2.6 V versus Li/Li^+ at different current densities. The characteristic charging and discharging voltage profiles are shown in Figure 4a. The cell exhibited a high reversible specific capacity of ~1350 mAh g^{-1} at the rate of 0.1 C (discharging or charging of full theoretical capacity in 10 h). There was modest increase in polarization accompanying the increase of charging/discharging rate (Figure 4a), indicating highly efficient kinetics of the electrode material. Reversible specific capacities at different current densities of 0.1, 0.2, 0.5, 1, and 2 C were ~1350, ~1200, ~1050, ~900, and ~700 mAh g^{-1}, respectively. Figure 4b shows the electrochemical performance of the battery for the first 100 cycles. After a slight capacity decay during the initial 3 cycles at 0.1 C, the reversible capacity of the Li–S battery stabilized at ~1350 mAh g^{-1} and then showed stable capacity retention at each charging/discharging rate up to 2 C with Coulombic efficiency higher than 99% (Figure 4b).

To assess long-term cycling performace of our ternary material, another cell using the CNT/$NiFe_2O_4$–S hybrid as the working electrode was first activated at the rates of 0.2 and 0.5 C for 30 cycles and then cycled at 1 C for 500 cycles (Figure 4c). Our CNT/$NiFe_2O_4$–S material showed extraordinary cycling stability. Specific capacity higher than 850 mAh g^{-1} could be retained after 500 recharging cycles, corresponding to capacity decay as low as 0.009% per cycle with excellent Coulombic efficiency higher than 99.2%. To our best knowledge, the result represents the highest cycling stability that has ever been achieved by S-based electrode materials under comparable measurement conditions (without additional cell configuration engineering such as applying an interlayer, Table S1).[13,16,19,22−24,27,28,33,39,40] After more than 500 cycles at 1 C, the same cell continued to be cycled at 2 C for another 150 cycles. A reversible capacity of ~690 mAh g^{-1} was observed, 98.1% of which was retained after the 150 cycles (Figure 4d), corresponding to a low capacity decay of 0.013% per cycle. After this extended cycling test, the morphology of CNT/$NiFe_2O_4$–S material was preserved (Figure S3). It was observed that the $NiFe_2O_4$ nanosheets were still anchored on the CNT framework. S was still well-embedded in the CNT/$NiFe_2O_4$ scaffold, as revealed by EDS mapping of the ternary hybrid material after more than 700 cycles (Figure 5). XRD measurement of the discharged material after hundreds of cycles excluded the possibility of $NiFe_2O_4$ evolving into other phases (Figure S4).

Discussion. The superior electrochemical performance of the CNT/$NiFe_2O_4$–S material, with respect to high specific capacity, good rate capability, and unprecedented cycling stability, is a direct result of the unique material structure. In the ternary hybrid architecture, there are three components playing irreplaceable roles and cooperating to deliver the excellent electrochemical performance.

DOI: 10.1021/jacs.5b07071
J. Am. Chem. Soc. 2015, 137, 12946−12953

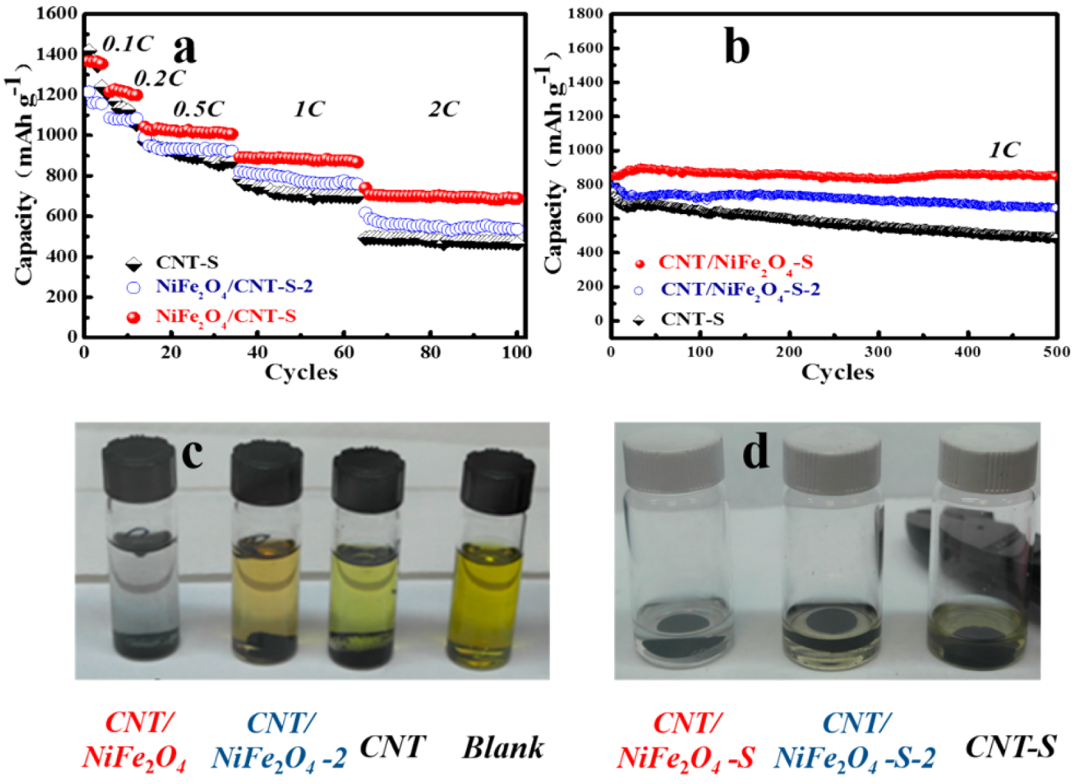

Figure 6. Influences of material structure and morphology on polysulfide confinement and battery cycling stability. (a) Comparison of electrochemical performance of S deposited on different host materials (CNT, CNT/$NiFe_2O_4$-2, and CNT/$NiFe_2O_4$). (b) Comparison of long-term cycling stability of S deposited on the different host materials. (c) Photo of the different host materials soaked in polysulfide solution. (d) Photo of the long-term cycled CNT/$NiFe_2O_4$−S, CNT/$NiFe_2O_4$−S-2, and CNT−S cathodes soaked in mixed DOL/DME solvent.

The CNTs wire the $NiFe_2O_4$ nanosheets and form a 3D porous network. The interwoven and highly conductive CNTs provide fast paths for electron transport during battery operation.[36,37,41] Electrons can be rapidly shuttled between the active material particles and the current collector through the CNT network, which allows for achievment of a high degree of S utilization to realize high specific capacity and fast electrochemical kinetics to enhance rate performance. The 3D porous structure also affords a large surface area for high sulfur loading and adequate relaxing space for alleviating the considerable volumetric changes during the charging/discharging processes of the S cathode.[37,42]

The $NiFe_2O_4$ nanosheets are the key component for adsorbing polysulfide intermediates and suppressing the shuttling effect during battery operation. The lithium polysulfides are highly polar species that lack strong interactions with the nonpolar CNTs. The polar surfaces of $NiFe_2O_4$ can strongly bind polysulfides via metal−sulfur interactions, which is essential for trapping the polysulfide intermediates and mitigating capacity decay during cycling. In a control experiment, the CNT−S binary hybrid material without a $NiFe_2O_4$ component showed much faster capacity fading during the first 100 cycles in spite of a higher initial capacity (Figure 6a). Interestingly, we also found that the S-adsorbing capability of $NiFe_2O_4$ appears to be morphology-dependent. The $NiFe_2O_4$ nanosheets confine polysulfides better than the $NiFe_2O_4$ nanoparticles, which is evidenced by the lower cycling stability for the first 100 cycles of another CNT/$NiFe_2O_4$−S hybrid material where the $NiFe_2O_4$ is in the form of nanoparticles (Figure 6a). From here on, the binary hybrid material with $NiFe_2O_4$ nanoparticles grown on CNTs (Figure S5) is denoted as CNT/$NiFe_2O_4$-2 to distinguish it from the CNT/$NiFe_2O_4$ material with $NiFe_2O_4$ nanosheets. The ternary material made by depositing S onto CNT/$NiFe_2O_4$-2 is named CNT/$NiFe_2O_4$−S-2 accordingly for clarity. The representative charging/discharging voltage profiles of the CNT−S and CNT/$NiFe_2O_4$−S-2 are shown in Figures S6 and S7, respectively. Figure 6b compares the long-term cycling stability of the CNT−S and CNT/$NiFe_2O_4$−S-2 control samples with that of the CNT/$NiFe_2O_4$−S material. After activation at low current densities, the CNT−S sample showed the worst cycling performance among the three, only maintaining 64.3% of the initial capacity after 500 cycles, corresponding to a large capacity decay of ∼0.0715% per cycle. Addition of an oxide component significantly improved the cycle life: The CNT/$NiFe_2O_4$−S-2 sample exhibited an average capacity decay of ∼0.0314% per cycle over 500 cycles, which was better than that of the CNT−S material but still worse than that of the CNT/$NiFe_2O_4$−S (0.009% per cycle) suggesting that the nanosheet-shaped $NiFe_2O_4$ is more effective in trapping polysulfide intermediates and stabilizing the charging/discharging process.

We performed adsorption experiments to compare the capability of the CNT/$NiFe_2O_4$ hybrid material in trapping polysulfides with both the CNT and CNT/$NiFe_2O_4$-2 samples, taking Li_2S_6 as the polysulfide representative that was prepared using a previously reported method.[13] An equivalent amount of each material was added to a fixed volume of solution containing a fixed amount of Li_2S_6 dissolved in DOL mixed with DME in a volumetric ratio of 1:1. The solution containing CNT/$NiFe_2O_4$ turned completely colorless (Figure 6c), indicating strong adsorption of Li_2S_6 by the solid. The solution containing CNT/$NiFe_2O_4$-2 was slightly colored (Figure 6c),

DOI: 10.1021/jacs.5b07071
J. Am. Chem. Soc. 2015, 137, 12946−12953

confirming that the $NiFe_2O_4$ nanoparticles have lower adsorption capacity for Li_2S_6 than do the $NiFe_2O_4$ nanosheets. The CNT solution was even darker in color (Figure 6c) because of the weak interaction of CNT with Li_2S_6. Such differences in adsorption capability explain well the observed different cycling performance of the corresponding materials in batteries. To test whether the CNT/$NiFe_2O_4$–S ternary structure can still effectively trap polysulfides after the long-term cycling test, the cycled cathode with absorbed electrolyte was directly soaked in a mixture of DOL/DME (1:1, vol). The solution remained colorless (Figure 6d), indicating that the polysulfides were still well-confined within the electrode structure rather than dissolved in electrolyte after the long-term cycling process.[29] In comparison, a yellow solution color from dissolved polysulfides was observed for both the CNT–S and CNT/$NiFe_2O_4$–S-2 electrodes after being soaked into the DOL/DME solvent. We found the CNT/$NiFe_2O_4$-2 has a specific surface area larger than that of the CNT/$NiFe_2O_4$ (300 vs 192 m^2/g), suggesting that the adsorption of polysulfides on $NiFe_2O_4$ surface is likely chemical in nature and possibly through the interactions between the negatively charged polysulfide anions and the positively charged metal cations. The morphology dependence may be attributed to the unique surface structures of the $NiFe_2O_4$ nanosheets, such as the geometric arrangement of the metal cations or their electronic states. Identification of the interaction sites and morphology-dependent adsorption mechanism still needs further investigation.

Finally, the S component of the CNT/$NiFe_2O_4$–S hybrid material is the active phase that stores and releases energy by Li^+ insertion and extraction. The S deposition method we adopted in the synthesis produced fine S nanoparticles that were well-distributed on the CNT/$NiFe_2O_4$ scaffold.[21] The small particle size shortens the diffusion length for Li^+ and electrons within the S active material as well as increases the reaction surface area, which facilitates the battery cycling reactions especially at high current density. The CNT/$NiFe_2O_4$ scaffold strongly anchors the S nanoparticle layer, leading to a high degree of S utilization. The resulting high reversible specific capacity and excellent Coulombic efficiency supports long cycle life.

SUMMARY AND CONCLUSIONS

We have demonstrated a novel design of a CNT/$NiFe_2O_4$–S ternary hybrid material structure that simultaneously addresses the electron conduction, lithium ion diffusion, and polysulfide dissolution/shuttling problems to boost the performance of the S cathode in Li–S batteries. In this unique material architecture, each component synergistically serves a specific purpose: The CNTs construct a 3D highly conductive porous network. The $NiFe_2O_4$ nanosheets strongly trap polysulfide intermediates. The small S nanoparticles enable fast Li^+ storage/release. All of these contribute to the high reversible specific capacity, good power rate, and excellent cycling stability. This discovery opens a path for employing multicomponent hybrid materials with rationally designed structures and functions to improve Li–S batteries.

ASSOCIATED CONTENT

Supporting Information

The Supporting Information is available free of charge on the ACS Publications website at DOI: 10.1021/jacs.5b07071.

Procedures and additional data. (PDF)

AUTHOR INFORMATION

Corresponding Author

*hailiang.wang@yale.edu

Notes

The authors declare no competing financial interest.

ACKNOWLEDGMENTS

This work was supported by Yale University. Q.F. acknowledges financial support from the International Postdoctoral Exchange Fellowship Program under grant no. 20140056 by China Postdoctoral Council and National Natural Science Foundation of China (51407029). We thank Prof. Fei Wei (Tsinghua University) for providing the CNTs, Ming Gong (Stanford University) for performing surface area measurements, and Julia Zhuang (Yale University) for proof reading the manuscript.

REFERENCES

(1) Armand, M.; Tarascon, J. M. *Nature* **2008**, *451*, 652.
(2) Van Noorden, R. *Nature* **2014**, *507*, 26.
(3) Cheng, F.; Liang, J.; Tao, Z.; Chen, J. *Adv. Mater.* **2011**, *23*, 1695.
(4) Bruce, P. G.; Freunberger, S. A.; Hardwick, L. J.; Tarascon, J.-M. *Nat. Mater.* **2011**, *11*, 19.
(5) Choi, N.–S.; Chen, Z.; Freunberger, S. A.; Ji, X.; Sun, Y.-K.; Amine, K.; Yushin, G.; Nazar, L. F.; Cho, J.; Bruce, P. G. *Angew. Chem., Int. Ed.* **2012**, *51*, 9994.
(6) Yang, Y.; Zheng, G.; Cui, Y. *Chem. Soc. Rev.* **2013**, *42*, 3018.
(7) Manthiram, A.; Chung, S.-H.; Zu, C. *Adv. Mater.* **2015**, *27*, 1980.
(8) Kim, J. H.; Fu, K.; Choi, J.; Kil, K.; Kim, J.; Han, X.; Hu, L.; Paik, U. *Sci. Rep.* **2015**, *5*, 8946.
(9) Chen, R.; Zhao, T.; Lu, J.; Wu, F.; Li, L.; Chen, J.; Tan, G.; Ye, Y.; Amine, K. *Nano Lett.* **2013**, *13*, 4642.
(10) Ji, X.; Lee, K. T.; Nazar, L. F. *Nat. Mater.* **2009**, *8*, 500.
(11) Hwa, Y.; Zhao, J.; Cairns, E. J. *Nano Lett.* **2015**, *15*, 3479.
(12) Zhang, S.; Ueno, K.; Dokko, K.; Watanabe, M. *Adv. Energy Mater.* **2015**, *5*, 1500117.
(13) Pang, Q.; Kundu, D.; Cuisinier, M.; Nazar, L. F. *Nat. Commun.* **2014**, *5*, 4759.
(14) Zheng, J.; Tian, J.; Wu, D.; Gu, M.; Xu, W.; Wang, C.; Gao, F.; Engelhard, M. H.; Zhang, J.-G.; Liu, J.; Xiao, J. *Nano Lett.* **2014**, *14*, 2345.
(15) Ji, X.; Evers, S.; Black, R.; Nazar, L. F. *Nat. Commun.* **2011**, *2*, 325.
(16) Wang, L.; Dong, Z.; Wang, D.; Zhang, F.; Jin, J. *Nano Lett.* **2013**, *13*, 6244.
(17) Wei Seh, Z.; Li, W.; Cha, J. J.; Zheng, G.; Yang, Y.; McDowell, M. T.; Hsu, P.-C.; Cui, Y. *Nat. Commun.* **2013**, *4*, 1331.
(18) Qiu, Y.; Li, W.; Zhao, W.; Li, G.; Hou, Y.; Liu, M.; Zhou, L.; Ye, F.; Li, H.; Wei, Z.; Yang, S.; Duan, W.; Ye, Y.; Guo, J.; Zhang, Y. *Nano Lett.* **2014**, *14*, 4821.
(19) Zhou, G.; Zhao, Y.; Manthiram, A. *Adv. Energy Mater.* **2015**, *5*, 1402263.
(20) Lu, S.; Cheng, Y.; Wu, X.; Liu, J. *Nano Lett.* **2013**, *13*, 2485.
(21) Chen, H.; Wang, C.; Dong, W.; Lu, W.; Du, Z.; Chen, L. *Nano Lett.* **2015**, *15*, 798.
(22) Wang, H.; Yang, Y.; Liang, Y.; Robinson, J. T.; Li, Y.; Jackson, A.; Cui, Y.; Dai, H. *Nano Lett.* **2011**, *11*, 2644.
(23) Xu, F.; Tang, Z.; Huang, S.; Chen, L.; Liang, Y.; Mai, W.; Zhong, H.; Fu, R.; Wu, D. *Nat. Commun.* **2015**, *6*, 7221.
(24) Kim, H.; Lee, J.; Ahn, H.; Kim, O.; Park, M. J. *Nat. Commun.* **2015**, *6*, 7278.
(25) Xin, S.; Gu, L.; Zhao, N.-H.; Yin, Y.-X.; Zhou, L.-J.; Guo, Y.-G.; Wan, L.-J. *J. Am. Chem. Soc.* **2012**, *134*, 18510.
(26) Ji, L.; Rao, M.; Zheng, H.; Zhang, L.; Li, Y.; Duan, W.; Guo, J.; Cairns, E. J.; Zhang, Y. *J. Am. Chem. Soc.* **2011**, *133*, 18522.
(27) Wang, Z.; Dong, Y.; Li, H.; Zhao, Z.; Bin Wu, H.; Hao, C.; Liu, S.; Qiu, J.; Lou, X. W. *Nat. Commun.* **2014**, *5*, 5002.

DOI: 10.1021/jacs.5b07071
J. Am. Chem. Soc. 2015, 137, 12946–12953

(28) Yao, H.; Zheng, G.; Hsu, P.-C.; Kong, D.; Cha, J. J.; Li, W.; Seh, Z. W.; McDowell, M. T.; Yan, K.; Liang, Z.; Narasimhan, V. K.; Cui, Y. *Nat. Commun.* **2014**, *5*, 3943.
(29) Xiao, Z.; Yang, Z.; Wang, L.; Nie, H.; Zhong, M. e.; Lai, Q.; Xu, X.; Zhang, L.; Huang, S. *Adv. Mater.* **2015**, *27*, 2891.
(30) Zhang, Q.; Wang, Y.; Seh, Z. W.; Fu, Z.; Zhang, R.; Cui, Y. *Nano Lett.* **2015**, *15*, 3780.
(31) Zhou, Y.; Zhou, C.; Li, Q.; Yan, C.; Han, B.; Xia, K.; Gao, Q.; Wu, J. *Adv. Mater.* **2015**, *27*, 3774−3781.
(32) Hart, C. J.; Cuisinier, M.; Liang, X.; Kundu, D.; Garsuch, A.; Nazar, L. F. *Chem. Commun.* **2015**, *51*, 2308.
(33) Liang, X.; Hart, C.; Pang, Q.; Garsuch, A.; Weiss, T.; Nazar, L. F. *Nat. Commun.* **2015**, *6*, 5682.
(34) Zhao, Y.; Wu, W.; Li, J.; Xu, Z.; Guan, L. *Adv. Mater.* **2014**, *26*, 5113.
(35) Zhao, M.-Q.; Peng, H.-J.; Tian, G.-L.; Zhang, Q.; Huang, J.-Q.; Cheng, X.-B.; Tang, C.; Wei, F. *Adv. Mater.* **2014**, *26*, 7051.
(36) Wang, H.; Liang, Y.; Gong, M.; Li, Y.; Chang, W.; Mefford, T.; Zhou, J.; Wang, J.; Regier, T.; Wei, F.; Dai, H. *Nat. Commun.* **2012**, *3*, 917.
(37) Wang, H.; Dai, H. *Chem. Soc. Rev.* **2013**, *42*, 3088.
(38) Wang, H. L.; Robinson, J. T.; Diankov, G.; Dai, H. J. *J. Am. Chem. Soc.* **2010**, *132*, 3270.
(39) Zhou, G.; Pei, S.; Li, L.; Wang, D.-W.; Wang, S.; Huang, K.; Yin, L.-C.; Li, F.; Cheng, H.-M. *Adv. Mater.* **2014**, *26*, 625.
(40) Song, J.; Gordin, M. L.; Xu, T.; Chen, S.; Yu, Z.; Sohn, H.; Lu, J.; Ren, Y.; Duan, Y.; Wang, D. *Angew. Chem.* **2015**, *127*, 4399.
(41) Fan, Q.; Lei, L.; Yin, G.; Sun, Y. *Chem. Commun.* **2014**, *50*, 2370.
(42) Peng, H.-J.; Huang, J.-Q.; Zhao, M.-Q.; Zhang, Q.; Cheng, X.-B.; Liu, X.-Y.; Qian, W.-Z.; Wei, F. *Adv. Funct. Mater.* **2014**, *24*, 2772.

DOI: 10.1021/jacs.5b07071
J. Am. Chem. Soc. 2015, 137, 12946−12953